How to cite: *Angew. Chem. Int. Ed.* **2020**, *59*, 17442–17446
International Edition: doi.org/10.1002/anie.202007210
German Edition: doi.org/10.1002/ange.202007210

Electroluminescence

Constructing Charge-Transfer Excited States Based on Frontier Molecular Orbital Engineering: Narrowband Green Electroluminescence with High Color Purity and Efficiency

Yincai Xu, Chenglong Li, Zhiqiang Li, Qingyang Wang, Xinliang Cai, Jinbei Wei,* and Yue Wang**

Abstract: *The design and synthesis of organic materials with a narrow emission band in the longer wavelength region beyond 510 nm remain a great challenge. For constructing narrowband green emitters, we propose a unique molecular design strategy based on frontier molecular orbital engineering (FMOE), which can integrate the advantages of a twisted donor–acceptor (D-A) structure and a multiple resonance (MR) delayed fluorescence skeleton. Attaching an auxiliary donor to a MR skeleton leads to a novel molecule with twisted D-A and MR structure characteristics. Importantly, a remarkable red-shift of the emission maximum and a narrowband spectrum are achieved simultaneously. The target molecule has been employed as an emitter to fabricate green organic light-emitting diodes (OLEDs) with Commission Internationale de L'Eclairage (CIE) coordinates of (0.23, 0.69) and a maximum external quantum efficiency (EQE) of 27.0 %.*

Thermally activated delayed fluorescence (TADF) molecules have been considered as one of the most promising emitting materials for organic light-emitting diodes (OLEDs) because they can harvest electro-generated triplet excitons for the emission of light and achieve a theoretical internal quantum efficiency (IQE) of 100 % by an efficient reverse intersystem crossing (RISC) process from the lowest triplet state (T_1) to the lowest singlet state (S_1).[1] A small singlet–triplet splitting energy (ΔE_{ST}) between the S_1 and T_1 is responsible for realization of RISC, which can be realized by minimizing the overlap between the highest occupied molecular orbital (HOMO) and the lowest unoccupied molecular orbital (LUMO) of organic molecules with spatially separated donor–acceptor (D-A) structures.[2] The often adopted strategy for generating molecular architectures for TADF is to construct a highly twisted D-A molecular skeleton with a significant intramolecular charge-transfer (ICT) characteristic, which can inevitably induce the generation of a large Stokes shift and a broad emission spectrum as a result of remarkable structure relaxation in the excited states.[3] For real-world display applications, emission spectra with broad bandwidths are extremely detrimental to achieve high color purity and cannot satisfy the requirement of wide color gamut displays.[4] For commercial OLED displays, although relatively narrow electroluminescence (EL) spectra with good color purity have been achieved by cutting off the margin region of the original broad EL spectra by using optical technologies such as color filters or microcavities, these treatments significantly result in an increase of power consumption and product cost.[5] However, a most significant advantage of a D-A molecule with a highly twisted structure is the relative ease of regulating the emission maximum, especially beyond $\lambda = 500$ nm.

Recently, it has been demonstrated that multiple resonance (MR) type B-N-containing TADF molecules, composed of a rigid skeleton with regular arrangements of boron and nitrogen atoms (Scheme 1 a), exhibit narrow emission bands and can be employed to fabricate highly efficient OLEDs with perfect color purity.[6] In the case of bis(*N*,*N*-diphenylamino)benzene (BDPAB) and 1,3-bis(carbazol-9-yl)benzene (BCAB) based MR-type TADF molecules,[6a–c] it

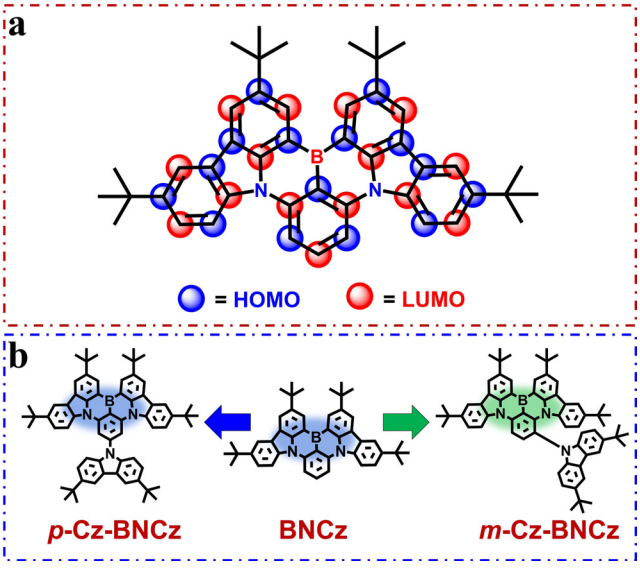

Scheme 1. a) The MR framework of BNCz. b) The molecular structures of *p*-Cz-BNCz, BNCz, and *m*-Cz-BNCz.

[*] Y. Xu, Dr. C. Li, Q. Wang, X. Cai, Dr. J. Wei, Prof. Y. Wang
State Key Lab of Supramolecular Structure and Materials
College of Chemistry, Jilin University
Changchun, 130012 (China)
E-mail: chenglongli@jlu.edu.cn
weijb12@mails.jlu.edu.cn
yuewang@jlu.edu.cn
Dr. Z. Li, Prof. Y. Wang
Jihua Laboratory
13 Nanpingxi Road, Foshan, 528200, Guangdong Province (China)
Supporting information and the ORCID identification number for one of the authors of this article can be found under: https://doi.org/10.1002/anie.202007210.

is relatively easy to synthesize blue and sky-blue triphenylboron-containing molecules with narrow full-width at half-maximum (FWHM) emission. However, constructing narrowband TADF emitters based on the above skeleton with emission maxima greater than 510 nm remains a great challenge. It is clear that although extending the conjugation length of BDPHAB or BCZB could result in longer wavelength emission, greater conjugation would induce the destruction of the HOMO and LUMO localization in the MR structure and lead to a broad emission. According to the standard of the National Television System Committee (NTSC), the fabrication of full color displays need not only narrowband deep-blue emitters but also ultrapure green ones with Commission Internationale de L'Eclairage (CIE) coordinates of (0.21, 0.71) and red ones with CIE coordinates of (0.67, 0.33). How to red-shift the BDPHAB- or BCZB-based MR emission maximum to around $\lambda = 530$ and 630 nm while simultaneously keeping a narrowband emission remain an unaddressed issue. There is an urgent demand for the development of a molecular design strategy for narrowband red, green, and blue emitters for practical applications in wide color gamut OLED displays. More importantly, the establishment of a molecular design and synthesis method for narrowband emission molecules is of great significance from the viewpoint of fundamental science.

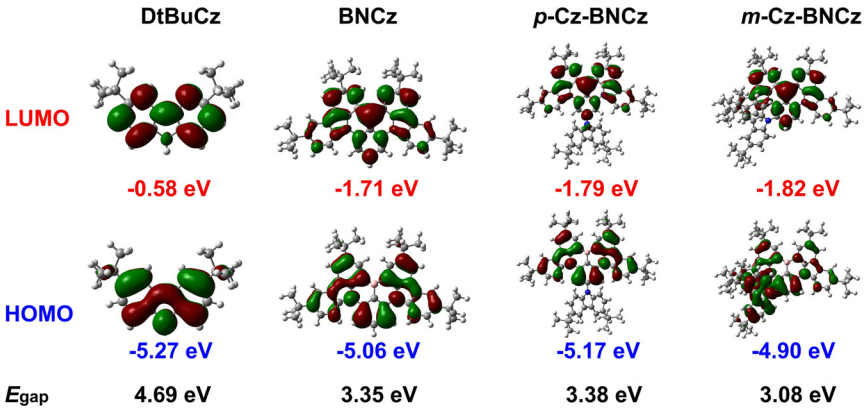

Figure 1. The HOMO and LUMO distributions a well as calculated energy gaps of DtBuCz, BNCz, *p*-Cz-BNCz, and *m*-Cz-BNCz.

In this context, we have combined the advantages of the spatially separated D-A structure and fused MR skeleton to synthesize pure green emitters with a narrowband width. Our approach is based on a basic idea of introducing an auxiliary electron-donor moiety into a HOMO-localized *meta*-carbon position relative to the B-substituted phenyl ring within the BCAB-based MR framework (Scheme 1b). Upon attaching an auxiliary 3,6-di-*tert*-butylcarbazole (DtBuCz) as a large and often used donor to a *meta*-carbon position, the HOMO energy level of the resulting molecule *m*-Cz-BNCz should increase significantly, while the LUMO energy level should change only slightly compared with the parent molecule BNCz (Scheme 1b), thereby resulting in a red-shift of the emission. The auxiliary donor DtBuCz and parent BNCz MR plane should adopt a twisted structure, since *meta*-substitution of DtBuCz would induce strong steric hindrance. The unique target molecule *m*-Cz-BNCz (Scheme 1b) should represent a perfect combination of twisted D-A structure and MR skeleton and enable a red-shifted emission and narrowband spectrum to be successfully achieved simultaneously.

Herein, we primarily selected the reported bluish-green emissive compound BNCz[6b–c] as a B-N-containing parent core skeleton and constructed *m*-Cz-BNBCz (for detailed synthesis and characterizations, see the Supporting Information and Figures S1–S4) by attaching DtBuCz as a donor group to the *meta*-carbon position relative to the B-substituted phenyl ring. Firstly, the ground-state (S_0) geometries and frontier molecular orbital distributions (Figure 1) of *m*-Cz-BNCz and BNCz as well as *p*-Cz-BNCz (Scheme 1b),[6b] which is the isomer of *m*-Cz-BNCz, were calculated using density functional theory (DFT). The configurations of *m*-Cz-BNCz and BNCz in the excited S_1 states were simulated using time-dependent DFT (TDDFT; Figures S5). *p*-Cz-BNCz and BNCz exhibit identical HOMO/LUMO distributions and similar energy levels, which suggests that *p*-substitution of DtBuCz has negligible influence on the emission properties of the parent molecule core. This is because the *para*-carbon atom relative to the B-substituted phenyl ring is localized by the LUMO and the DtBuCz group, as an electron donor attached to it cannot be involved in the frontier molecular orbital of the BNCz core. Significantly, the LUMO of *m*-Cz-BNCz is identical to that of BNCz, while its HOMO is the combination of the HOMOs of BNCz and DtBuCz (Figure 1 and Figure S6). The introduction of DtBuCz at the *meta*-carbon position of BNCz results in the HOMO of *m*-Cz-BNCz being formed by the direct combination of the HOMOs of BNCz and DtBuCz. The HOMO energy level of *m*-Cz-BNCz exhibits a remarkable increase, thereby suggesting a notable red-shift of the emission. A comparison of the photoluminescence (PL) spectra (Figure S7) of BNCz, *p*-Cz-BNCz, and *m*-Cz-BNCz reveals that *para*-substitution of DtBuCz induces a slight blue-shift of the emission while *meta*-substitution results in a clear red-shift of the emission, which strongly supports our molecular design idea. Therefore, the proposed strategy based on frontier molecular orbital engineering (FMOE) is efficient. The dihedral angle between the proximal *meta*-substituted *tert*-butylcarbazole donor and the B-substituted phenyl ring is 51.4° (Figure S8), indicative of a twisted D-A structure. The separated HOMO–LUMO distributions can enhance the ICT characteristic of *m*-Cz-BNCz and reduce the energy gap (E_{gap}) between the frontier molecular orbitals, which is benefical for a red-shifted emission. The calculated dipole moments for the optimized S_0 geometries of BNCz and *m*-Cz-BNCz are 0.31 and 0.90 Debye, respectively. The corresponding dipole moments for BNCz and *m*-Cz-BNCz in the optimized S_1 geometries are 3.75 D and 8.73 D, respectively. The much larger change in the dipole moments of the excited state further confirms the

enhanced ICT property of *m*-Cz-BNCz. Most importantly, *m*-Cz-BNCz shows a narrowband emission.

Based on cyclic voltammetry (CV) measurements (Figure S9), the HOMO and LUMO energy levels of *m*-Cz-BNCz are estimated to be −5.15 and −2.63 eV, respectively. The measured HOMO and LUMO energy levels for BNCz are −5.40 and −2.61 eV, respectively. The experimental results agree well with the theoretically calculated values. *m*-Cz-BNCz shows excellent thermal stability with a high decomposition and/or sublimation temperature ($T_{d/s}$, corresponding to 5% weight loss) of 403 °C (Figure S10), which is sufficient for the vacuum thermal deposition process for OLED fabrication. The preliminary photophysical properties of *m*-Cz-BNCz were characterized in dilute toluene solution (1×10^{-5} M; Figure 2 and Table S1). The UV/Vis absorption spectrum displays an intense absorption band that reaches a maximum at 484 nm, which is ascribed to the ICT absorption transition. In solution at room temperature, *m*-Cz-BNCz shows vivid green fluorescence with an emission maximum at $\lambda = 519$ nm, a small Stokes shift of 35 nm, and a narrow FWHM of 38 nm. Notably, the solid-state PL spectrum of *m*-Cz-BNCz closely resembles that recorded in toluene solution. This finding suggests this molecule displays negligible aggregation-induced shifting of the emission and broadening behaviors, which indicates that the intermolecular interactions of the compound are efficiently inhibited owing to the highly twisted molecular structure. Additionally, *m*-Cz-BNCz exhibits stronger positive solvatochromism and solvent-dependent spectral profile characteristics compared with BNCz (Figure S11 and Table S2), thereby demonstrating the enhanced ICT property of *m*-Cz-BNCz. This phenomenon coincides well with the theoretically calculated results. Furthermore, the absolute photoluminescence quantum yield (PLQY) measured with an integer-sphere system in oxygen-free toluene solution is as high as 97%. The ΔE_{ST} value was calculated to be 0.08 eV from the onsets of the low-temperature fluorescence and phosphorescence spectra at 77 K (Figure S12). Such a small ΔE_{ST} value is favorable for exciton upconversion from T_1 to S_1 and thus gives rise to efficient TADF emission.

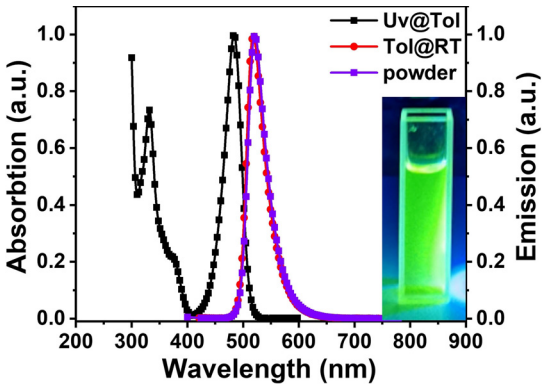

Figure 2. The normalized UV/Vis absorption and fluorescence spectra of *m*-Cz-BNCz measured in toluene solution (1×10^{-5} M, 298 K) and the corresponding powder fluorescence spectrum. (inset: photograph in toluene taken under 365 nm UV light).

To further elucidate the TADF nature of *m*-Cz-BNCz, the temperature-dependent transient PL spectra of the doped thin film of 1 wt% *m*-Cz-BNCz:PhCzBCz (PhCzBCz = 9-(2-(9-phenyl-9*H*-carbazol-3-yl)phenyl)-9*H*-3,9′-bicarbazole) were investigated (Figure S13a). Upon increasing the temperature from 80 to 330 K, the ratio of the delayed component from the recursive $S_1 \rightarrow S_0$ transition by successive upconversion of triplet excitons increases gradually, indicative of a typical TADF nature. At room temperature, the doping concentration dependent photophysical characterizations (Figure S14 and Table S3 and S4) of *m*-Cz-BNCz:PhCzBCz films reveal that increasing the doping concentration from 1 wt% to 50 wt% results in only a slight change in the PLQY values (94 ± 2%), which suggests that the aggregation-induced emission quenching is efficiently suppressed. Uniquely, the *m*-Cz-BNCz:PhCzBCz films exhibit much shorter delayed fluorescence lifetimes (τ_d; Figure S13b) of less than one microsecond (μs) compared with reported B-N-containing MR compounds with τ_d of several tens of microseconds.[6a–i] The short τ_d values are conducive to the fast RISC process of *m*-Cz-BNCz in the films, and in combination with the large rate constants of fluorescence (k_F: $>6.0\times10^7$ s^{-1}), which can efficiently alleviate the concentration quenching of triplet excitons in electroluminescent devices, suppresses the efficiency roll-off with the increase of brightness.[7] For all the doped films, the rate constants of RISC (k_{RISC}) are around 1.0×10^6 s^{-1}, which suggests an efficient $T_1 \rightarrow S_1$ exciton upconversion, which is beneficial for the utilization of more excitons. The delayed lifetime gradually decreased as the dopant concentration was increased, which may be attributed to the fact that the triplet–triplet annihilation (TTA) induced excited-state quenching is stronger in films with a high dopant concentration. Theoretical calculations demonstrate that *m*-Cz-BNCz has a much larger spin-orbital coupling (SOC) constant of 0.154 cm^{-1} compared with that of BNCz (0.028 cm^{-1}) and *p*-Cz-BNCz (0.014 cm^{-1}; Table S5), suggesting that *m*-Cz-BNCz should have a shorter τ_d value.

To evaluate the EL performance of *m*-Cz-BNCz as an emitter, multilayer OLEDs with an optimized device configuration of [ITO/TAPC (50 nm)/TCTA (5 nm)/PhCzBCz:*x* wt% *m*-Cz-BNCz (30 nm)/TmPyPB (30 nm)/LiF (0.8 nm)/Al (100 nm)] were fabricated ($x = 1$, 3, 5, 10, 20, 30, 50), where PhCzBCz was used as the host to form an emitting layer (EML) with *m*-Cz-BNCz, while TAPC (1,1-bis[(di-4-tolylamino)phenyl]cyclohexane) and TmPyPB (3,3′-[5′-[3-(3-pyridinyl)phenyl][1,1′:3′,1″-terphenyl]3,3″diyl]bis-pyridine) were adopted as the hole transporting layer (HTL) and electron transporting layer (ETL), respectively. To prevent excitons from diffusing into the TAPC layer, TCTA (tris(4-carbazolyl-9-ylphenyl)amine) was employed as an exciton blocking layer (EBL). The energy level diagram of the device and the molecular structures of the materials used are shown in Figure S15. The detailed device parameters are summarized in Table 1.

All the devices displayed a low turn-on voltage that gradually decreased from 3.1 V to 2.6 V as the *m*-Cz-BNCz doping concentration was increased from 1 to 50 wt% (Figure S16a). This finding suggests that, at higher doping concentration, carriers tend to be injected directly into *m*-Cz-

Table 1: Summary of the electroluminescent data of the *m*-Cz-BNCz-based devices.

x wt%	$\lambda^{[a]}$ [nm]	FWHM[b] [nm]	V_{on}[c] [V]	L_{max}[d] [cd m^{-2}]	CE_{max}[e] [cd A^{-1}]	PE_{max}[f] [lm W^{-1}]	EQE[g] [%]	CIE (*x*, *y*)[h]
1	520	43	3.1	15820	96.4	97.7	26.8/22.9/11.9	(0.22, 0.68)
3	520	44	3.0	25590	99.2	103.9	27.0/24.2/14.4	(0.23, 0.69)
5	524	44	3.0	25750	102.2	107.1	27.4/25.7/16.4	(0.24, 0.69)
10	528	45	2.9	26230	117.6	127.4	31.4/29.0/17.5	(0.26, 0.68)
20	528	45	2.9	23100	112.5	117.8	29.8/27.8/17.0	(0.26, 0.68)
30	528	47	2.7	22200	103.6	120.5	27.3/25.4/15.7	(0.28, 0.67)
50	528	48	2.6	17980	103.6	117.0	27.0/25.2/13.6	(0.29, 0.67)

[a] EL maximum wavelength. [b] Full width at half maximum. [c] Turn-on voltage at 1 cd m^{-2}. [d] Maximum luminance. [e] Maximum current efficiency. [f] Maximum power efficiency. [g] Maximum external quantum efficiency and values at 100 and 1000 cd m^{-2}. [h] Value at 100 cd m^{-2}.

BNCz dopant rather than through PhCzBCz matrix.[8] All the devices emit green light and increasing the dopant concentration results in a slight red-shift of the emission maxima from $\lambda = 520$ to 528 nm and an unremarkable improvement of the FWHM values from 43 to 48 nm (Figure 3). The best CIE coordinates of (0.23, 0.69) and a high maximum external quantum efficiency (EQE) of 27.0% were achieved at a 3 wt% doping concentration. These values are extremely close to the standard green-light CIE coordinates of (0.21, 0.71) stipulated by the NTSC and represent the best green emitter among the TADF materials reported to date (Figure S17).[6b–c,9] In addition, the device exhibited good spectra stability over a wide range of driving voltages from 3 to 8 V (Figure S18).

The device with a 10 wt% doping concentration displays the maximum EQE, current efficiency (CE), and power efficiency (PE) of 31.4%, 117.6 cd A^{-1}, and 127.4 lm W^{-1} (Figures S16b and S19), respectively, which is comparable with the reported efficiencies for the high-performance phosphorescence-based green OLEDs.[10] The high device efficiency principally originates from the very fast RISC process and high fluorescent radiative efficiency ($S_1 \rightarrow S_0$ transition) for *m*-Cz-BNCz. When the doping concentration exceeds 10 wt%, the maximum EQE decreases gradually. Intriguingly, the *m*-Cz-BNCz-based devices all display high maximum EQEs of over 26.8% within a wide range of doping concentrations from 1 to 50 wt%, which suggests that the highly twisted structure of *m*-Cz-BNCz can efficiently suppress the emission quenching at high doping concentrations. The performances of *m*-Cz-BNCz-based devices, including their highly pure green color, remarkable EQEs, and insignificant concentration-dependent property, convincingly demonstrate that our molecular design approach for constructing precious-metal-free EL materials is efficient.

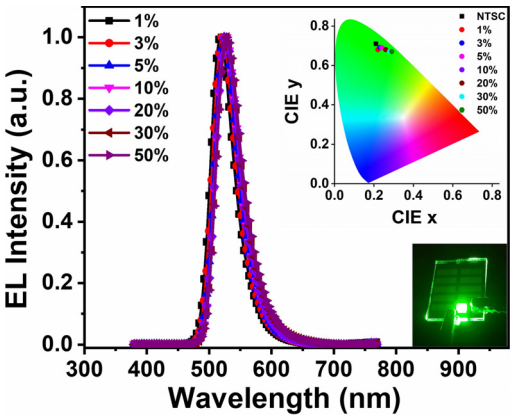

Figure 3. EL spectra of the devices. (inset: The color coordinates of the devices on the CIE 1931 color space and the photograph showing the emission color of the device at 3 wt% doping concentration).

In conclusion, we proposed a unique molecular design idea for constructing highly efficient TADF emitters with narrow luminescent spectra, which can be employed to develop high-performance EL material with high color purity. By precisely introducing an auxiliary donor group to the HOMO-distributed carbon atom of a MR skeleton, the resulting molecule was endowed with a twisted D-A structure. The perfect combination between twisted D-A structure and MR skeleton provide an efficient method to develop TADF materials with emission maxima in the longer wavelength region and a narrowband width. As a result, we showed a facile molecular synthesis strategy to achieve TADF materials with an emission maximum beyond 520 nm and a narrow FWHM, which was beneficial to achieve highly efficient full-color EL materials with perfect color purity. In this study, we presented a molecule *m*-Cz-BNCz that exhibited ultrapure green EL with CIE coordinates of (0.23, 0.69) and a maximum EQE of 27.0%. The use of FMOE may be of importance to guide the exploration of more ultrahigh color purity TADF materials in the longer wavelength region and pave the way towards future practical wide color gamut displays.

Acknowledgements

This work was supported by the National Natural Science Foundation of China (21935005 and 51803069) and the National Key R&D Program of China (2016YFB0401000).

Conflict of interest

The authors declare no conflict of interest.

Keywords: donor–acceptor structures · electroluminescence · green emission · organic light-emitting diodes · thermally activated delayed fluorescence

[1] a) H. Uoyama, K. Goushi, K. Shizu, H. Nomura, C. Adachi, *Nature* **2012**, *492*, 234 – 238; b) C. W. Tang, S. A. VanSlyke, *Appl. Phys. Lett.* **1987**, *51*, 913 – 915; c) Y. Tao, K. Yuan, T. Chen, P. Xu, H. Li, R. Chen, C. Zheng, L. Zhang, W. Huang, *Adv. Mater.* **2014**, *26*, 7931 – 7958; d) Z. Yang, Z. Mao, Z. Xie, Y. Zhang, S. Liu, J. Zhao, J. Xu, Z. Chi, M. P. Aldred, *Chem. Soc. Rev.* **2017**, *46*, 915 – 1016; e) X. Y. Cai, S.-J. Su, *Adv. Funct. Mater.* **2018**, *28*, 1802558.

[2] a) X.-K. Chen, Y. Tsuchiya, Y. Ishikawa, C. Zhong, C. Adachi, J.-L. Brédas, *Adv. Mater.* **2017**, *29*, 1702767; b) P. L. Dos Santos, J. S. Ward, D. G. Congrave, A. S. Batsanov, J. Eng, J. E. Stacey, T. J. Penfold, A. P. Monkman, M. R. Bryce, *Adv. Sci.* **2018**, *5*, 1700989; c) K. Wu, T. Zhang, Z. Wang, L. Wang, L. Zhan, S. Gong, C. Zhong, Z. H. Lu, S. Zhang, C. Yang, *J. Am. Chem. Soc.* **2018**, *140*, 8877 – 8886; d) Y.-J. Shiu, Y.-C. Cheng, W.-L. Tsai, C.-C. Wu, C.-T. Chao, C.-W. Lu, Y. Chi, Y.-T. Chen, S.-H. Liu, P.-T. Chou, *Angew. Chem. Int. Ed.* **2016**, *55*, 3017 – 3021; *Angew. Chem.* **2016**, *128*, 3069 – 3073; e) X.-L. Chen, J.-H. Jia, R. Yu, J.-Z. Liao, M.-X. Yang, C.-Z. Lu, *Angew. Chem. Int. Ed.* **2017**, *56*, 15006 – 15009; *Angew. Chem.* **2017**, *129*, 15202 – 15205; f) J. Huang, H. Nie, J. Zeng, Z. Zhuang, S. Gan, Y. Cai, J. Guo, S. J. Su, Z. Zhao, B. Z. Tang, *Angew. Chem. Int. Ed.* **2017**, *56*, 12971 – 12976; *Angew. Chem.* **2017**, *129*, 13151 – 13156; g) J. W. Sun, J.-H. Lee, C.-K. Moon, K.-H. Kim, H. Shin, J.-J. Kim, *Adv. Mater.* **2014**, *26*, 5684 – 5688; h) I. S. Park, K. Matsuo, N. Aizawa, T. Yasuda, *Adv. Funct. Mater.* **2018**, *28*, 1802031; i) S. J. Zou, F. M. Xie, M. Xie, Y. Q. Li, T. Cheng, X. H. Zhang, C. S. Lee, J. X. Tang, *Adv. Sci.* **2020**, *7*, 1902508.

[3] F. Santoro, A. Lami, R. Improta, J. Bloino, V. Barone, *J. Chem. Phys.* **2008**, *128*, 224311.

[4] a) X. Li, Y. Z. Shi, K. Wang, M. Zhang, C. J. Zheng, D. M. Sun, G. L. Dai, X. C. Fan, D. Q. Wang, W. Liu, Y. Q. Li, J. Yu, X. M. Ou, C. Adachi, X. H. Zhang, *ACS Appl. Mater. Interfaces* **2019**, *11*, 13472 – 13480; b) Y. Yuan, X. Tang, X. Y. Du, Y. Hu, Y. J. Yu, Z. Q. Jiang, L. S. Liao, S. T. Lee, *Adv. Opt. Mater.* **2019**, *7*, 1801536; c) D. Hall, S. M. Suresh, P. L. dos Santos, E. Duda, S. Bagnich, A. Pershin, P. Rajamalli, D. B. Cordes, A. M. Z. Slawin, D. Beljonne, A. Köhler, I. D. W. Samuel, Y. Olivier, E. Zysman-Colman, *Adv. Opt. Mater.* **2020**, *8*, 1901627.

[5] a) T.-Y. Cho, C.-L. Lin, C.-C. Wu, *Appl. Phys. Lett.* **2006**, *88*, 111106; b) D. Poitras, C.-C. Kuo, C. Py, *Opt. Express* **2008**, *16*, 8003 – 8015; c) N. Takada, T. Tsutsui, S. Saito, *Appl. Phys. Lett.* **1993**, *63*, 2032.

[6] a) T. Hatakeyama, K. Shiren, K. Nakajima, S. Nomura, S. Nakatsuka, K. Kinoshita, J. Ni, Y. Ono, T. Ikuta, *Adv. Mater.* **2016**, *28*, 2777 – 2781; b) Y. Zhang, D. Zhang, J. Wei, Z. Liu, Y. Lu, L. Duan, *Angew. Chem. Int. Ed.* **2019**, *58*, 16912 – 16917; *Angew. Chem.* **2019**, *131*, 17068 – 17073; c) Y. Xu, Z. Cheng, Z. Li, B. Liang, J. Wang, J. Wei, Z. Zhang, Y. Wang, *Adv. Opt. Mater.* **2020**, *8*, 1902142; d) Y. Kondo, K. Yoshiura, S. Kitera, H. Nishi, S. Oda, H. Gotoh, Y. Sasada, M. Yanai, T. Hatakeyama, *Nat. Photonics* **2019**, *13*, 678 – 682; e) S. H. Han, J. H. Jeong, J. W. Yoo, J. Y. Lee, *J. Mater. Chem. C* **2019**, *7*, 3082 – 3089; f) K. H. Lee, J. Y. Lee, *J. Mater. Chem. C* **2019**, *7*, 8562 – 8568; g) J. A. Knöller, G. Meng, X. Wang, D. Hall, A. Pershin, D. Beljonne, Y. Olivier, S. Laschat, E. Zysman-Colman, S. Wang, *Angew. Chem. Int. Ed.* **2020**, *59*, 3156 – 3160; *Angew. Chem.* **2020**, *132*, 3181 – 3185; h) X. Liang, Z. P. Yan, H. B. Han, Z. G. Wu, Y. X. Zheng, H. Meng, J. L. Zuo, W. Huang, *Angew. Chem. Int. Ed.* **2018**, *57*, 11316 – 11320; *Angew. Chem.* **2018**, *130*, 11486 – 11490; i) S. Oda, B. Kawakami, R. Kawasumi, R. Okita, T. Hatakeyama, *Org. Lett.* **2019**, *21*, 9311 – 9314; j) K. Matsui, S. Oda, K. Yoshiura, K. Nakajima, N. Yasuda, T. Hatakeyama, *J. Am. Chem. Soc.* **2018**, *140*, 1195 – 1198; k) S. Nakatsuka, H. Gotoh, K. Kinoshita, N. Yasuda, T. Hatakeyama, *Angew. Chem. Int. Ed.* **2017**, *56*, 5087 – 5090; *Angew. Chem.* **2017**, *129*, 5169 – 5172.

[7] C. Murawski, K. Leo, M. C. Gather, *Adv. Mater.* **2013**, *25*, 6801 – 6827.

[8] H. Kaji, H. Suzuki, T. Fukushima, K. Shizu, K. Suzuki, S. Kubo, T. Komino, H. Oiwa, F. Suzuki, A. Wakamiya, Y. Murata, C. Adachi, *Nat. Commun.* **2015**, *6*, 8476.

[9] a) P. Rajamalli, N. Senthilkumar, P. Gandeepan, P. Y. Huang, M. J. Huang, C. Z. Ren-Wu, C. Y. Yang, M. J. Chiu, L. K. Chu, H. W. Lin, C. H. Cheng, *J. Am. Chem. Soc.* **2016**, *138*, 628 – 634; b) T.-L. Wu, M.-J. Huang, C.-C. Lin, P.-Y. Huang, T.-Y. Chou, R.-W. Chen-Cheng, H.-W. Lin, R.-S. Liu, C.-H. Cheng, *Nat. Photonics* **2018**, *12*, 235 – 240; c) Y. J. Cho, K. S. Yook, J. Y. Lee, *Adv. Mater.* **2014**, *26*, 6642 – 6646; d) C. Tang, T. Yang, X. Cao, Y. Tao, F. Wang, C. Zhong, Y. Qian, X. Zhang, W. Huang, *Adv. Opt. Mater.* **2015**, *3*, 786 – 790; e) A. E. Nikolaenko, M. Cass, F. Bourcet, D. Mohamad, M. Roberts, *Adv. Mater.* **2015**, *27*, 7236 – 7240.

[10] a) C.-H. Shih, P. Rajamalli, C.-A. Wu, M.-J. Chiu, L.-K. Chu, C.-H. Cheng, *J. Mater. Chem. C* **2015**, *3*, 1491 – 1496; b) H.-H. Chou, C.-H. Cheng, *Adv. Mater.* **2010**, *22*, 2468 – 2471.

Manuscript received: May 18, 2020
Accepted manuscript online: June 12, 2020
Version of record online: August 6, 2020

